



Self-powered microfluidic device for the colorimetric detection of lithium via sequential reagent mixing

Angelo Traina, Han J.G.E. Gardeniers, Burcu Gumuscu

Online Publication Date: 05 Apr 2021

URL: <http://www.jresm.org/archive/resm2021.251ma0125.html>

DOI: <http://dx.doi.org/10.17515/resm2021.251ma0125>

Journal Abbreviation: *Res. Eng. Struct. Mater.*

To cite this article

Traina A, Gardeniers HJGE, Gumuscu B. Self-powered microfluidic device for the colorimetric detection of lithium via sequential reagent mixing. *Res. Eng. Struct. Mater.*, 2021; 7(3): 347-360.

Disclaimer

All the opinions and statements expressed in the papers are on the responsibility of author(s) and are not to be regarded as those of the journal of Research on Engineering Structures and Materials (RESM) organization or related parties. The publishers make no warranty, explicit or implied, or make any representation with respect to the contents of any article will be complete or accurate or up to date. The accuracy of any instructions, equations, or other information should be independently verified. The publisher and related parties shall not be liable for any loss, actions, claims, proceedings, demand or costs or damages whatsoever or howsoever caused arising directly or indirectly in connection with use of the information given in the journal or related means.



Published articles are freely available to users under the terms of Creative Commons Attribution - NonCommercial 4.0 International Public License, as currently displayed at [here](https://creativecommons.org/licenses/by-nc/4.0/) (the "CC BY - NC").



Self-powered microfluidic device for the colorimetric detection of lithium via sequential reagent mixing

Angelo Traina^{1,2,a}, Han J.G.E. Gardeniers^{1,b}, Burcu Gumuscu^{1,3,4,c}

¹Mesoscale Chemical Systems Group, University of Twente, Enschede, The Netherlands

²Department Information Engineering, Electronics and Telecommunications, Sapienza University of Rome, Rome, Italy

³BioInterface Science Group, Eindhoven University of Technology, Eindhoven, The Netherlands

⁴Biosensors and Devices Group, Eindhoven University of Technology, Eindhoven, The Netherlands

Article Info

Article history:

Received 25 Jan 2021

Revised 19 Mar 2021

Accepted 31 Mar 2021

Keywords:

Lithium detection;
Colorimetric detection;
Microfluidic circuits;
Finger-driven pump

Abstract

Continuous monitoring of lithium concentration fluctuations in blood plasma is essential for patients with bipolar disorder and manic depression since lithium has a low therapeutic index. While blood plasma concentrations between 0.4 and 1.0 mmol/L are considered to be in the therapeutic zone, the concentrations exceeding 1.3 mmol/L are toxic to the patients. Most of the point-of-care devices for lithium monitoring have bulky peripherals and require extensive operator handling, yet simple-to-use devices are in demand for 2–5% of the worldwide population receiving lithium therapy. This paper aims to develop a self-contained microfluidic device to run colorimetric lithium assays without the need for dedicated personnel or equipment. In the developed microchip, the assay reagents are mixed in sequential order via custom-designed microfluidic capillary circuits with the aid of a finger pump. The operation of the finger pump was characterized mathematically and demonstrated experimentally. The finger-driven pump achieved 45.9 mm/s flow velocity when 8.3 μ L liquid was placed in a 160 mm long channel with 200 μ m height, as such rapid triggering was a requirement for the colorimetric lithium test. The final device is able to quantify the lithium concentrations between 0 and 2.0 mM using a smartphone camera. The detection limit of this microchip was calculated as 0.1 mM. This device presents a portable alternative to on-site quantitative detection techniques with bulky and expensive tools.

© 2021 MIM Research Group. All rights reserved.

1. Introduction

Lithium is used as a mood stabilizer medication in clinics. Patients with bipolar disorders and recurrent depression often are prescribed lithium salts for treatment, although the administration of lithium bears its risks. While lithium levels below 0.1 mmol/L do not pose an effective treatment, levels above 1.3 mmol/L can lead to toxic effects on critical organs including the brain, liver, and kidneys. [1-3] Currently lithium monitoring in patients is predominantly based on laborious and time-consuming laboratory testing techniques. Therefore, the development of alternative measurement techniques that can be used in resource-limited settings would be of great benefit. The World Health Organization (WHO) requires that newly developed diagnostic measurement tools should be “assured”; in other words, they should be affordable, sensitive, specific, user-friendly, rapid and robust, equipment-free, and deliverable to end-users. [4] The availability of

*Corresponding author: b.gumuscu@tue.nl

^a<https://orcid.org/0000-0001-5374-8360>; ^borcid.org/0000-0003-0581-2668;

^corcid.org/0000-0003-4843-4724

DOI: <http://dx.doi.org/10.17515/resm2021.251ma0125>

Res. Eng. Struct. Mat. Vol. 7 Iss.2 (2021) 347-360

“assured” diagnostic tools is the key to future scalability in terms of the number of users that can be reached, thus facilitating a convenient therapy for the patients.

Blood testing has been the workhorse of lithium monitoring since alternative approaches, such as urine or saliva readings, do not give reliable results. [5] The standard laboratory tests to detect lithium from blood include colorimetry [6], photometry [7], and atomic absorption spectroscopy [8]. A more recent technique is called thermal ionization ion mobility spectrometry, which detected lithium from serum samples by following the steps of vaporization, ionization and separation while traveling in a weak electric field under atmospheric pressure. [9] All of these techniques require dedicated equipment and an operator with suitable expertise. The demand for more accessible and straightforward ways to monitor lithium levels in blood has motivated the development of microfluidic tools. For example, a rapid test was developed based on the photometric reading of a microcuvette, where the colorimetric reaction takes place upon the mixing of plasma-separated blood and a pre-loaded colorimetric reagent has been introduced. [10] Capillary electrophoresis-based measurements were also employed using whole blood in disposable chips, which perform conductivity measurements for lithium content determination. [11-14] Paper-based microfluidics platforms and lateral-flow devices. [15, 16] Recently, the group of Tokeshi introduced a paper-based device for lithium detection which is achieved by folding absorbent papers for different steps of the process, involving blood separation, and colorimetric detection. [17] Another paper-based platform was developed to run potentiometric measurements from serum using solid-state ion-selective electrodes for lithium. [18] For the sophisticated capillarity-driven networks, colorimetric [19] and electrochemical [20] detection of lithium were also demonstrated without the use of an external pump. In a recent work, a self-powered pump was demonstrated by the group of Basabe-Desmonts, who created large-area PDMS micropumps with microfluidic cartridges produced by multilayer lamination of grafted plastic substrates. [21] All these devices paved the way towards advanced lithium detection tests, although problems associated with affordability, user-friendliness, and robustness of the platforms still need to be tackled.

This work presents a self-contained microfluidic platform that exploits the capabilities of conventional microfluidic devices with capillary networks. The platform can handle the suction of a large volume of liquid with high flow rates to be used for point-of-care analysis, which can be performed by the non-experts (e.g. patients). This work involves the following: (1) the working mechanism of the sequential liquid delivery and finger pump operation were explained theoretically, (2) design and fabrication of the microfluidic device and the finger pump were demonstrated, (3) an on-chip colorimetric assay for lithium quantification was demonstrated as a proof-of-concept demonstration. The platform operates with small volumes of liquids and no external supporting equipment or power because liquid movement in the platform is controlled by a finger pump and capillarity. This work opens new avenues for the control of lithium administration of patients and the implementation of self-contained analytical platforms in resource-limited settings.

2. Theory

2.1. Operation of capillary circuits for sequential liquid delivery

To understand the behaviour and estimate the performance of the developed microfluidic system, a theoretical model based on an equivalent fluidic circuit concept was constructed and solved numerically. The model is based on the Navier-Stokes equation (1):

$$\rho(\vec{v} \cdot \nabla) \vec{v} = -\nabla\rho + \eta\nabla^2 \vec{v} + F \tag{1}$$

where \vec{v} is the velocity field [m s⁻¹], which is a distribution of velocity in a given region, and is denoted by $\vec{v} = \vec{v}(\vec{r}, t)$, ρ is the fluid density [kg m⁻³]; η is the dynamic viscosity [Pa s]; F represents any external forces present [N]. Analogous to electrical resistance, fluid resistance is defined as the ratio of pressure drop over flow rate in Equation (2):

$$R = \frac{\Delta p}{Q} \tag{2}$$

where Δp is the applied pressure difference [N m⁻²], and Q is the volume flow rate [m³ s⁻¹]. Under the hypothesis of a channel with a rectangular shape with width w ; length L ; height h ; laminar flow; unidirectional motion; integrating Equation (1), Equation (3) is obtained:

$$Q \approx \frac{h^3 w \Delta p}{12 \eta L} \left(1 - 0.630 \frac{h}{w} \right) \tag{3}$$

$$R = \frac{12 \eta L}{1 - 0.630 \left(\frac{h}{w} \right)} \frac{1}{h^3 w} \tag{4}$$

Equation (4) leads to important observations: (i) the pressure drop through a channel is proportional to the volumetric flow rate and the hydraulic resistance, where the local pressure drop in the section considered determines the volumetric flow rate and not the overall pressure drop. (ii) The hydraulic resistance R remains constant for a specific fluid as long as the geometry of the channel is fixed, and under these assumptions, proportional to the channel length L . All these parameters are fundamental in the design of our microfluidic device, which requires accurate control in terms of volume, channel filling times and functionalization of the reaction chambers.

The theoretical principle behind the operation of the capillary stop valves has been described in detail by Zimmermann et al [22]. The stop valves halt the flow of liquid in microchannels without external intervention, but using a sharp change in channel width creates a pressure barrier. The pressure barrier (ΔP) for a two dimensional stop valve is given by Equation (5):

$$P = -\gamma \left(\frac{\cos \theta_t + \cos \theta_b}{h} + \frac{\cos \theta_r + \cos \theta_l}{w} \right) \tag{5}$$

where w, h are the width and height respectively of the microchannel leading into the stop valve, and γ is the surface tension of the liquid. $\theta_t, \theta_b, \theta_r, \theta_l$, are the top, bottom, right, left channel wall contact angles. A numerical analysis was performed assuming that the liquid (reagent solution) advancement is stopped by an abrupt change in channel profile, due to the presence of the stop valves. Under these conditions the pressure in each channel junction P_n will be equal to the pressure exerted by the finger pump P_{max} . The reason is that the pressure generated by the pump is larger than the capillary pressure of the sides branches (Fig.1a), the liquid will be delivered from each branch to the channel junction P_n . To achieve a correct emptying of the i_{th} reservoir without activating the $R_{BV_{i+1}}$, it is essential to respect the condition at all times as shown in Equation (6):

$$|P_n| < |P_{i+1}| \tag{6}$$

where P_{i+1} with $i = 1, 2, 3$ is the capillary pressure at $(i+1)_{th}$ branches, R_{BV} is the resistance of one side branch; and P_n can be calculated using Kirchhoff's law and Ohm's law yielding Equation (7):

$$P_n = \frac{P_i \cdot R_C + P_{FP}(R_{SV} + R_i)}{(R_C + R_{RV} + R_i)} \tag{7}$$

where R_i is the series resistance between the R_{BV} and the reservoir resistance of each branch; R_{SV} is the resistance of the stop valve; R_C is the flow resistance of the colorimetric chamber.

2.2. Finger pump working principle

Under the assumptions of negligible gas leakage during the push-and-release process and constant temperature, it is possible to apply the ideal gas law using the geometric characteristics of the pump, as shown in Equation (8).

$$P_{max} = \left(\frac{V_0}{V_{min}} - 1 \right) P_0 \tag{8}$$

where P_{max} is the pressure increase when the pressure chamber is fully deformed [Pa]; P_0 is atmospheric pressure [Pa]; V_0 is the volume of the pressure chamber in its original shape [L]; V_{min} is the remaining volume of the pressure chamber when it is maximally deformed [L]. The volume of drawn fluid in the microchannel is closely related to the volumetric capacity of the finger pump. Thus, the movement of the liquids in the microchannels can be controlled by changing the volume of the finger pump or by modulating the applied force, without any external pressure units.

3. Materials and Methods

3.1. Materials

Poly(dimethylsiloxane) (PDMS) was purchased from Dow Silicones Deutschland GMBH (Theingaustr, DE), and SU8-50 negative photoresist was obtained from MicroChem, Corp. (Newton, MA). The colorimetric reaction designed for the quantification of lithium levels in biological fluids (ab235613 Lithium Assay Kit) was obtained from Abcam (Cambridge, GB).

3.2. Fabrication of the microfluidic device

The microfluidic network was developed to accommodate the pre-programmed delivery of multiple liquids sequentially for improved assay sensitivity and specificity in lithium sensing. The self-contained platform consists of two functional parts: a microfluidic network and a finger pump to trigger the mixing of colorimetric reaction solutions and blood plasma. Sequential liquid delivery was made possible by the stop valves that use an abrupt change in channel geometry and hydrophobic channel walls made of PDMS. The volume of microchannels scales with the solution volumes described in Abcam lithium test kit. Accordingly, 200 μm high microchannels with width and height 1000 μm x 26 000 μm , 1000 μm x 20 900 μm , 1000 μm x 200 μm and 800 μm x 1300 μm were designed, respectively. The width and height of the stop valves were 288 μm x 734 μm , respectively (Fig. 1a).

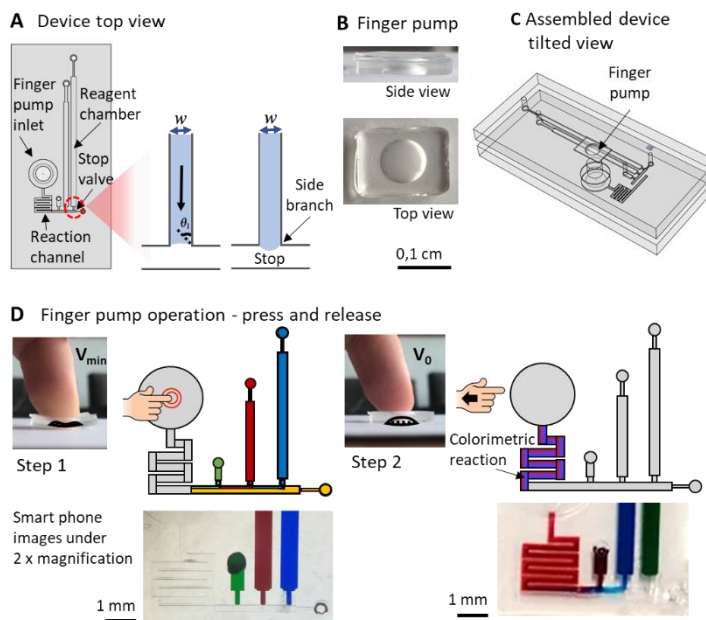


Fig. 1 (a) Device top view and its components. The stop valves are the T-junctions composed of two side branches. (b) Finger pump side and top views. (c) Assembled microchip with finger pump on top, finger pump, not to scale. (d) Finger pump operation is shown both in schematics and smartphone camera images.

The PDMS-based microfluidic device was fabricated using soft lithography. For the SU-8 mould preparation, a negative photoresist (MicroChem NANOTM SU-8 5) was spin-coated on a 4 inch silicon wafer, with a height of 200 μm , then baked on a hot plate at 95 $^{\circ}\text{C}$. The baked photoresist was exposed to ultraviolet (UV) light with a dose of 12m W cm^{-2} for 5 sec. For the post-exposure baking, the wafer was baked at 50 $^{\circ}\text{C}$ for 1 min, 65 $^{\circ}\text{C}$ for 1 min and 80 $^{\circ}\text{C}$ for 2 min, respectively. The wafer was cooled down to room temperature with steps of 5 $^{\circ}\text{C}$ per 2 min. The baked photoresist was developed with RER600 solvent (PGMEA RER600, ARCH chemicals) for 3.5 min with a spray-gun. The slow cooling down steps helped to minimize the thermal stress on the photoresist, and reduced the possibility of crack formation based on material stress.

The microfluidic chips were fabricated using the SU-8 mould. A PDMS mixture (10 : 1 w/w ratio of the polymer base to the curing agent) was poured onto the SU-8 mould. The PDMS mixture was cured for 2 h at 65 $^{\circ}\text{C}$ and peeled off from the SU-8 mould after curing. Several inlet and outlet holes were punched using biopsy punches with 1 mm and 4 mm diameter. Finally, the PDMS layer was bonded with a clean glass slide using oxygen plasma treatment for 45 sec. The final chip was placed in an oven set at 65 $^{\circ}\text{C}$ for 1 h (Figure S1a).

3.3. Design and Fabrication of The Finger Pump

The finger-driven pump was designed to drive the liquids in the microfluidic device. The finger pump is a deformable pressure chamber that was made of PDMS (Fig. 1b,c). Before the operation, positive pressure was applied on the finger pump via a human finger to deform it downwards. After this step, the finger pump was placed on the outlet of the device. Upon releasing the finger, the PDMS chamber deformed upwards and created a negative pressure inside the microchannels to trigger the liquid flow. This operation is based on the energy stored in the form of elastic energy inside the finger pump, as

described in Equation 8. The liquid movement stops when the PDMS pump restores its original shape. The inner volume of the microchip was calculated to be approximately 16 μL and the finger pump had a total volume of 100 μL that can be provided with the necessary suction (Fig. 1d).

The finger pump was fabricated using a master mould made by drilling an aluminium plate at the technical workshop at the University of Twente. The PDMS mixture (10 : 1 w/w ratio of the polymer base to the curing agent) was poured into the mould and cured at 65 °C in an oven for 1 h. The cured PDMS was peeled off from the mould (Fig. S1b). The distance covered by the liquid in the microchannels was measured by processing the smartphone images using Fiji software.

3.4. Colorimetric Lithium assay

Lithium Assay Kit manufacturer's guidelines were followed to quantitatively detect the lithium levels in blood plasma. After preparing the standards and the samples, sodium masking solution, lithium assay buffer, probe solution were mixed in microfluidic sequentially. After incubation of the solutions for 5 min, the microchannels were imaged using a smartphone camera attached to a 2x magnification lens. For the magenta intensity measurements, Fiji software was used to extract magenta values from the smartphone images, where a blank measurement was done using an unfilled channel. The images were taken under uniform light, sourced by a white LED lamp attached to 2x magnification lens. For the absorbance measurements, the samples were measured at 540 nm and 630 nm separately, using a microplate reader (Thermo Fisher Scientific Multiskan Go, Netherlands). The ratio of the two absorbance measurements is used to accurately determine the lithium concentration in the sample or the standard. The colorimetric reaction relies on a lithium-selective bi-chromatic probe molecule which is subjected to change absorbance at two distinct wavelengths upon binding to lithium ($\lambda_1 = 540 \text{ nm}$, $\lambda_2 = 630 \text{ nm}$). The probe molecule is found in the probe solution. Sodium masking solution is used for eliminating the interference by supra-physiological levels of serum sodium. Other mono-, di-, and trivalent ions found in the blood plasma do not interfere with the assay. Finally, the magenta values were compared with absorbance values.

4. Results and Discussion

As the key advance, the presented device is self-contained and no longer requires external parts such as electrodes, power source, syringe pumps unlike the previously reported tools.

4.1. Design of the Microfluidic Platform, Flow Channels and Capillary Circuits

The microfluidic system was designed for the quantification of lithium levels via four parallel microfluidic channels connected via a vertical microchannel, where the colorimetric reaction took place. The parallel microfluidic channels were emptied in sequential order to ensure the mixing of reagents in a correct order to achieve the most reliable results. The microchip had five inlets; three of the inlets were used to introduce reaction reagents, one inlet to introduce the sample via an integrated filter paper, and one inlet to connect the system to a finger pump (Fig. 1c). We considered the total resistance of each branch forming the microfluidic network when designing such a network of microchannels, where sequential delivery of a different amount of liquids was performed. Fig. 2a demonstrates a circuit model of the microfluidic network, consisting of stop valves, flow resistor, inlets, and microfluidic pump. Despite the complexity of the model, the stop valve was the component that mainly influences the flow, playing a key role in the sequential delivery.

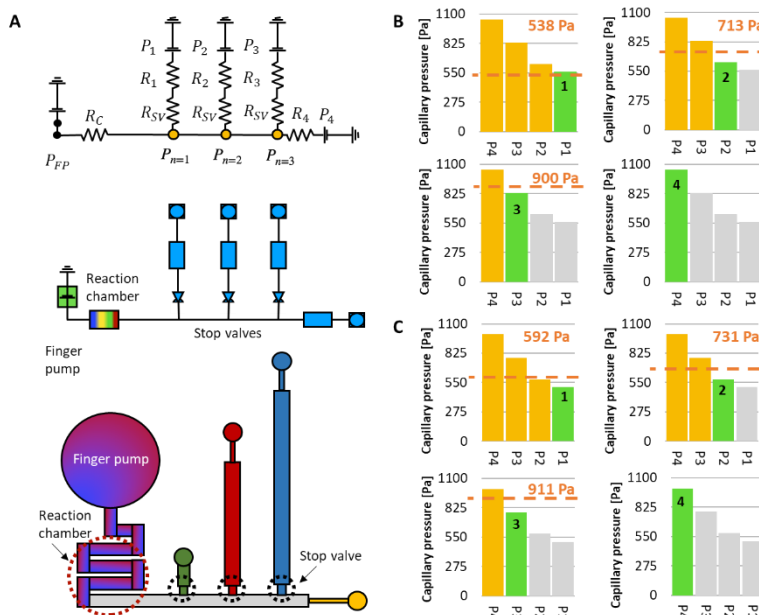


Fig. 2 (a) Symbolic and schematic representations and relative electric circuit analogue of microfluidic device propose. (b-c) Graphs show which reservoirs empty (in red) according to the sequential order for different surface contact angles $\theta = 89^\circ$ in (b) and $\theta = 95^\circ$ in (c). The numbers on green bars show the emptying order of the chambers shown in (a). Orange dashed lines show the pressure generated by the finger pump.

The microfluidic network was tested to understand how the geometry of stop valves influences their capacity of stopping the flow, and then sequentially releasing the liquid. Junker et al. [23] confirmed a success rate of 75% ($n = 8$) using a stop valve with $w = 200 \mu\text{m}$; $h = 734 \mu\text{m}$; and $\Delta h = 400 \mu\text{m}$ (height difference between stop valves and release channel). Our design involved interconnected four reservoirs with 8.6, 7.3, 0.8, 0.3 μL , respectively. The height of the channels were kept the same due to fabrication limitations while the width and length of the channels were changed to obtain the desired volumes. This resulted in an increase in resistance in the reservoirs of each branch, making the fulfilment of the condition in Equation (6) more difficult.

Figure 2b and 2c show the results of the numeric analysis of hydrophobic ($\theta > 90^\circ$) and hydrophilic ($\theta < 90^\circ$) contact angles characteristic to PDMS and glass surfaces [24-26], where the orange dotted line represents the pressure value P_n according to Equation (7). In either case, it was possible to find a numeric solution for the model by changing the geometry parameters (w ; L) of each reservoir. In this way, the sequential mixing of different reagents was obtained by fixing the channel height to $200 \mu\text{m}$. In this way, liquid advancement was not observed while loading the long reagent microchannels. In some cases, the finger pump operation caused the emptying of the microchannels not in a sequential order. This was attributed to the high width-to-height ratio of the stop valves. Nevertheless, the experimental findings support the numerical analysis that was obtained by the sequential emptying of the microchannels according to the anticipated order, with a success rate of 70% ($n = 15$). These results are in accordance with the work by Olanrewaju et al. [27].

The pressure drop was calculated in the total system by linking each channel parallel to each other. The microchip was composed of several PDMS layers and the variations in layer thickness directly affected the success rate of the sequential mixing. Although the finger-driven pump had 6.25 times more capacity to withdraw the solutions in the microchannels, the poor alignment of layers occasionally resulted in narrower connection channels between the layers, resulting in higher resistance at the connection locations.

4.2. Finger Pump

The finger pump was designed to accommodate fluid flow in microchannels and the dimensions were selected accordingly. To quantify the relationship between the size of the finger pump and the total microchannel volume, PDMS pressure chamber units were tested using two microchannels with different dimensions ($w_1 = 300 \mu\text{m}$, $w_2 = 600 \mu\text{m}$, $L = 160 \text{ mm}$, $h = 200 \mu\text{m}$) that are compatible with the final inner volume of the actual microchip design for colorimetric lithium monitoring. Figure 3a shows the microchips and the attached finger pump unit.

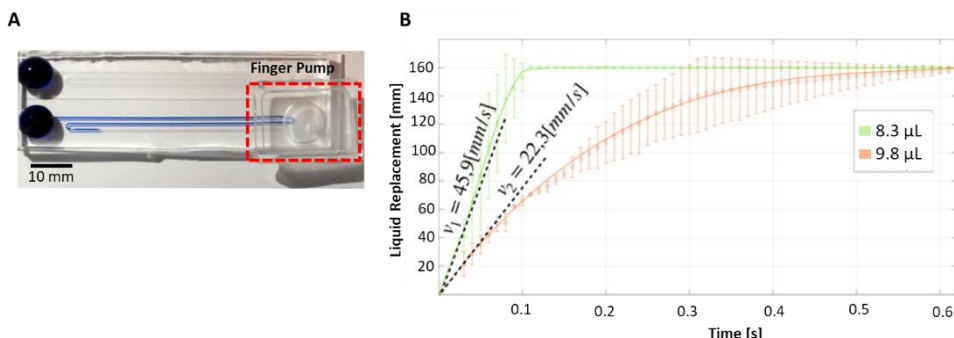


Fig. 3 The finger-driven pump induces fluid flow rate that is dependent on liquid volume in the microfluidic channels. (a) The finger-driven pumping system used for the characterization of the fabricated finger-driven pump with a diameter of 10 mm. (b) Liquid replacement by the micropump as a function of the time. Green and orange lines present the instant speed of the liquid in microchannels. The error bars in the graph show three separate measurements performed for this operation, $n = 3$.

For each width three emptying tests were ran using the finger pump. The selected diameter of the finger pump unit was sufficient to trigger the fluid flow in microchannels when fully deformed downwards. This finding matches the predicted behaviour described in Equation 8.

When microchannels were loaded with a larger volume of liquid ($V_1 = 9.8 \mu\text{L}$), the liquid reached the outlet in $\Delta t_1 = 0.64 \text{ s}$, without breaking up of the liquid slug in the microfluidic channels. As shown in Figure 3b, the acceleration of the liquid follows the second law of dynamics as shown in Equation (9):

$$a = \frac{dv}{dt} = \frac{F_{tot}}{m} \tag{9}$$

where m is the mass of liquid; a the acceleration applies to liquid.

When a fixed force, such as suction, is applied, a liquid mass in a microchannel gains speeds inversely proportional to its mass. Accordingly, the movement of the liquid mass was

calculated for $0 < t < 0.03$ s, by assuming that the mass m constantly accelerates, as shown in Equation (10).

$$\left\{ \begin{array}{l} a = a_0 \approx \frac{\Delta v}{\Delta t} = \frac{v_{fin} - v_{start}}{t_{fin} - t_{start}} \rightarrow \frac{v_{0.03}}{t_{0.03}} \\ v_{fin} = v_{start} + at \rightarrow v_{0.03} = 0 + a_0 t_{0.03} \\ x_{fin} = x_{start} + v_{start}t + \frac{1}{2}at^2 \rightarrow x_{0.03} = 0 + 0 \cdot t_{0.03} + \frac{1}{2}a_0 t_{0.03}^2 \end{array} \right. \quad (10)$$

The variations of acceleration are based on the variations in the mass of the liquid moved in the microchannel, so the liquid with a lower mass will have a higher speed in this range. Analogously, a smaller volume of liquid $V_2 = 8.3 \mu\text{L}$ was expected to accelerate slower than the larger volume $V_1 = 9.8 \mu\text{L}$ in the time frame $0 < t < 0.03$ s. Our observations in Figure 3b support this argument. The average velocity was calculated in each case as $v_1 = 2.3 \text{ mm/s}$ and $v_2 = 45.9 \text{ mm/s}$. We attribute the 2-fold velocity increase for $1.5 \mu\text{L}$ volume difference between the liquid masses to the possibility of unequal applied forces at each push and release cycle. These findings are in agreement with the findings of Xiang et al [25], as the finger pump successfully triggered fluid flow in microchannels with 160 mm length in 0.6 s.

The presented finger pump can trigger the fluid flow in a non-linear manner for shorter durations of time when compared to other self-powered microfluidic pumps in the literature. [26] Some of these pumps appear in the form of long and shallow microfluidic channels connected to a main channel, where the liquid suction takes place when the microchip is placed in a degassing chamber. In-parallel microchannels achieved a maximum suction velocity of 0.9 mm/s for when 1 mm to 3 mm diameter trenches were used. [21,28] The finger pump presented in this study is capable of triggering 20 to 40 times greater flow velocities for significantly longer microchannels. Another type of suction mechanism is based on paper-based microfluidics, where an absorbent fibrous paper is attached to the end of the microchannels. The liquid suction takes place due to capillary suction towards the absorbent material. In this manner, sequential mixing was made possible. The typical flow rates generated in such studies vary between 0.2 mm/s [29], and 0.2 to 0.1 $\mu\text{L/s}$ [27]. The flow rates generated by the finger pump were 80 times greater than these values, although the paper-driven pumps can function for longer time spans (tens of minutes) when compared to under 5 min operation of the finger driven pump presented in this work. Either way could be of preference as a requirement of different applications.

4.3. Colorimetric lithium assay

The main aim of this research was to develop a low-cost point-of-care device that allows for colorimetric detection of lithium using a smartphone camera in a rapidly and cost-effectively. Before the analysis of the specimens with unknown concentrations, the performance of the device for colour sensitivity was evaluated by standard specimens. The results of the colorimetric assay were captured for different lithium concentrations ranging between 0 and 2 mM using a smartphone camera (iPhone X, 12 MP camera). The concentration of lithium was correlated with the colour intensity in the white-balanced images. As described in the manufacturer’s datasheet, the associated change in colour from orange to red indicated the quantity of lithium inside the sample. Such a strategy was also previously followed by Tokeshi’s group. [17] To analyse how the variation in the concentration of lithium is connected to the absorbance value, the magenta values of the smartphone camera images and absorbance readouts were compared. Figure 4a demonstrates that the absorbance value, magenta value and lithium concentration have a linear relationship between 0 and 2 mM with a limit of detection of 0.1 mM ($n = 5$,

$R^2 = 0.99$). This test is capable of detecting various concentrations of lithium quantitatively, and the detection range covers the typical maximum and minimum concentrations of lithium in blood serum [30-35]. Figures 4b and 4c show the colour change in the reaction channel where the magenta values were extracted using MATLAB and Fiji software. The obtained results were found to be in correlation although the images obtained from the microchip were more faint compared to the ones in the off-chip measurement.

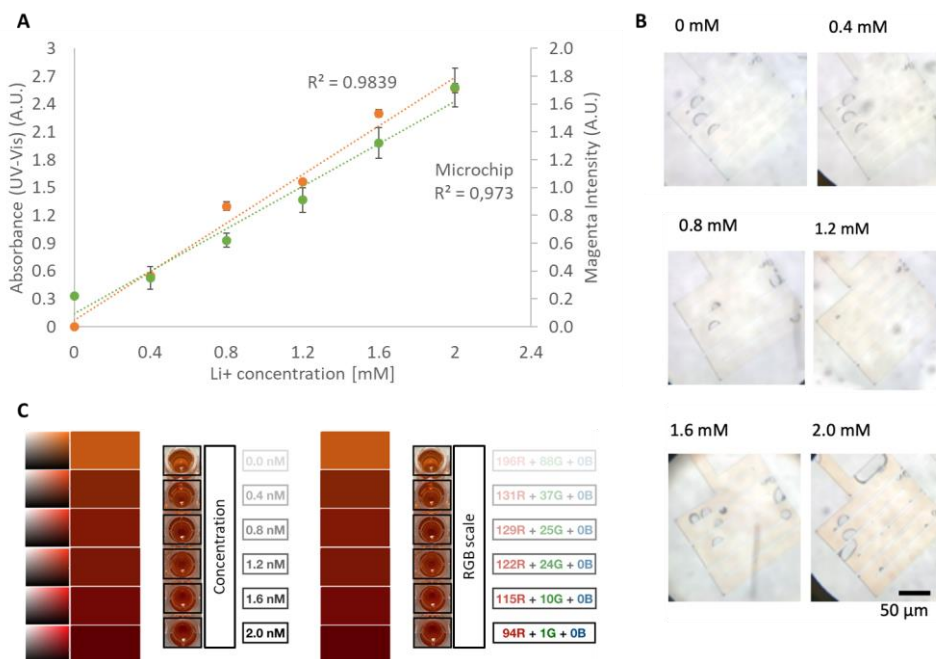


Fig. 4 (a) The quantitative calibration curve of different lithium concentrations for smartphone camera images (magenta only) and absorbance results. (b) On-chip assessment of the colorimetric reaction. Smartphone images of colorimetric detection of lithium in microchannels. (c) Off-chip correlation of the colorimetric reaction with RGB scale. The same methodology was followed to convert the detected colours on-chip.

5. Conclusions

We report here for the first time on the design, fabrication, and application of a self-standing device consisting of capillary microfluidic circuits for sequential mixing of reagents and a finger-driven pump for facilitating the fluid flow. As a proof-of-colorimetric lithium assay was performed in the device. The finger pump generated 20 to 40 times high flow rates when compared to the self-standing pumps reported in recent publications, while the pump operation time could be maintained in the range of minutes instead of hours as demonstrated in the previous studies. Nevertheless, the application selected for this work requires rapid mixing of reagents within minutes to start the colorimetric reaction. Therefore, the platform serves well to the aim of this work. The presented device meets the Affordability, Sensitivity, Specificity, User-friendliness, and Robustness (ASSURed) criteria requested by the World Health Organization (WHO). In this work, the request of the WHO was addressed by the two-pronged design of the self-powered microfluidic platform: First, in contrast to widely-used conductivity measurements, the platform requires no external electronic apparatus to run the lithium test. Second, the

proposed platform enables the mixing of reagents in a sequential order thanks to the finger-driven pump.

The finger pump assisted microfluidic system was designed and fabricated by using soft lithography. As a proof-of-concept study, a commercially available lithium kit was utilized to run the colorimetric lithium detection. The colorimetric reaction in the device occurred within 5 min after installing the reagents. A smartphone camera facilitated the image acquisition where colorimetric reaction detection was performed. The performance of the pump and liquid movement in microfluidic channels were characterized, and sequential emptying of the injected solutions. The detection limit of lithium concentration was measured to be 0.1 mmol/L. Our merging of rapid colorimetric lithium monitoring test with a stand-alone microfluidic device surmounts measurement challenges where (1) the measurement requires conductivity measurements, (2) there is the trade-off between the requirement of sequential mixing of reagents and assay sensitivity. The future work involves the implementation of a smartphone application, using the smartphone as a capture device and colour detector from a picture of the microfluidic device; and running the tests in spiked blood serum samples.

Acknowledgments

We thank all the Mesoscale Chemical Systems Lab members at the University of Twente for helpful discussions and suggestions throughout the study. We thank Stefan Schlautmann for helping with the production of the SU-8 moulds.

Annotations

\vec{v}	the velocity field
ρ	the fluid density
η	the dynamic viscosity
F	external forces
Δp	the applied pressure difference
Q	the volume flow rate
ΔP	the pressure barrier
R	the hydraulic resistance
L	the channel length
w	the width of the microchannel
h	the height of the microchannel
γ	the surface tension of the liquid
$\theta_t, \theta_b, \theta_r, \theta_l$	the top, bottom, right, left channel wall contact angles, respectively
P_n	the channel junction
P_{max}	the maximum pressure exerted by the finger pump

i^{th}	the number of the reservoirs
P_{i+1}	the capillary pressure at $(i+1)^{\text{th}}$ branches
R_{BV}	the resistance of one side branch;
R_i	the series resistance between the R_{BV} and the reservoir resistance of each branch
R_{SV}	the resistance of the stop valve
R_C	the flow resistance of the colorimetric chamber
P_0	the atmospheric pressure
V_0	the volume of the pressure chamber in its original shape
V_{min}	the remaining volume of the pressure chamber when it is maximally deformed
m	the mass of liquid
a	the acceleration that applies to liquid

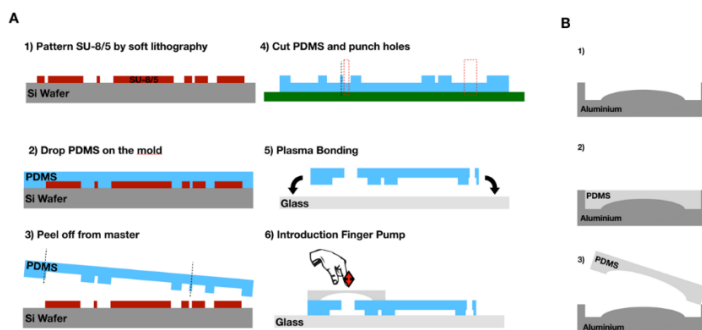
References

- [1] Hopkins S, Gelenberg J. Serum lithium levels and the outcome of maintenance therapy of bipolar disorder. *Bipolar Disorder*, 2000; 2: 174-179. <https://doi.org/10.1034/j.1399-5618.2000.020304.x>
- [2] Christian GD, Reagents for lithium electrodes and sensors for blood serum analysis. *Sensors*, 2002; 2: 432-435. <https://doi.org/10.3390/s21000432>
- [3] Reddy DS, Reddy MS. Serum lithium levels: Ideal time for sample collection! Are we doing it right?. *Indian Journal of Psychological Medicine.*, 2014; 36: 346-7. <https://doi.org/10.4103/0253-7176.135399>
- [4] Kosack CS, Page AL, Klatser PR. A guide to aid the selection of diagnostic tests. *Bulletin of the World Health Organization*, 2017; 95: 639. <https://doi.org/10.2471/BLT.16.187468>
- [5] Shetty SJ, Desai PB, Patil NM, Nayak RB. Relationship between serum lithium, salivary lithium, and urinary lithium in patients on lithium therapy. *Biological Trace Element Research.*, 2012; 147: 59-62. <https://doi.org/10.1007/s12011-011-9295-3>
- [6] Gruson D, Lallali A, Furlan V, Taburet AM, Legrand A, Conti M. Evaluation of a new lithium colorimetric assay performed on the Dade Behring Dimension® X-pand™ system. *Clinical Chemistry and Laboratory Medicine*, 2004; 42: 1066-1068. <https://doi.org/10.1515/CCLM.2004.214>
- [7] Christenson RH, Mandichak JJ, Duh SH, Augustyn JM, Thompson JC. Clinical performance characteristics of a new photometric lithium assay: a multicenter study. *Clinica Chimica Acta*, 2003; 327: 157-164. [https://doi.org/10.1016/S0009-8981\(02\)00367-4](https://doi.org/10.1016/S0009-8981(02)00367-4)
- [8] Rumbelow B, Peake M, Performance of a novel spectrophotometric lithium assay on a routine biochemistry analyser. *Annals of Clinical Biochemistry*, 2001; 38: 684-686. <https://doi.org/10.1258/0004563011900894>

- [9] Parchami R, Tabrizchi M, Shahraki H, Moaddeli A. Rapid analysis of lithium in serum samples by thermal ionization ion mobility spectrometry. *International Journal for Ion Mobility Spectrometry*, 2020; 23:117-25. <https://doi.org/10.1007/s12127-020-00264-1>
- [10] Glazer WM, Sonnenberg JG, Reinstein MJ, Akers RF. A novel, point-of-care test for lithium levels: description and reliability. *Journal of Clinical Psychiatry*, 2004; 65: 652-655. <https://doi.org/10.4088/JCP.v65n0508>
- [11] Vrouwe EX, Lutge R, Vermes I, Van Den Berg A. Microchip capillary electrophoresis for point-of-care analysis of lithium. *Clinical Chemistry*, 2007; 53: 117-123. <https://doi.org/10.1373/clinchem.2007.073726>
- [12] Floris A, Staal S, Lenk S, Staijen E, Kohlheyer D, Eijkel J, van den Berg, A. A prefilled, ready-to-use electrophoresis based lab-on-a-chip device for monitoring lithium in blood. *Lab on a Chip*, 2010; 10: 1799-1806. <https://doi.org/10.1039/c003899g>
- [13] Bidulock AC, Dubský P, van den Berg A, Eijkel J. Integrated internal standards: A sample prep-free method for better precision in microchip CE. *Electrophoresis*, 2019; 40: 756-765. <https://doi.org/10.1002/elps.201800393>
- [14] Sewart R, Gärtner C, Klemm R, Schattschneider S, Becker H. Microfluidic device for fast on-site biomedical diagnostic on the example of lithium analysis in blood. *Biomedical Engineering/Biomedizinische Technik*, 2012; 57(SI-1 Track-L): 729-732. <https://doi.org/10.1515/bmt-2012-4212>
- [15] Comer JP. Semiquantitative specific test paper for glucose in urine. *Analytical Chemistry*, 1956; 28: 1748-1750. <https://doi.org/10.1021/ac60119a030>
- [16] Gaikwad PS, Banerjee R. Advances in point-of-care diagnostic devices in cancers. *Analyst*, 2018; 143:1326-48. <https://doi.org/10.1039/c7AN01771E>
- [17] Komatsu T, Maeki M, Ishida A, Tani H, Tokeshi M. Based Device for the Facile Colorimetric Determination of Lithium Ions in Human Whole Blood. *ACS Sensors*. 2020; 5:1287-94. <https://doi.org/10.1021/acssensors.9b02218>
- [18] Novell M, Guinovart T, Blondeau P, Rius FX, Andrade FJ. A paper-based potentiometric cell for decentralized monitoring of Li levels in whole blood. *Lab on a Chip*, 2014; 14: 1308-1314. <https://doi.org/10.1039/c3lc51098k>
- [19] Martinez AW, Phillips ST, Carrilho E, Thomas SW, Sindi H, Whitesides GM. Simple telemedicine for developing regions: camera phones and paper-based microfluidic devices for real-time, off-site diagnosis. *Analytical Chemistry*, 2008; 80: 3699-707. <https://doi.org/10.1021/ac800112r>
- [20] Nie Z, Deiss, F, Liu X, Akbulut O, Whitesides GM. Integration of paper-based microfluidic devices with commercial electrochemical readers. *Lab on a Chip*, 2010; 10: 3163-3169. <https://doi.org/10.1039/c0lc00237b>
- [21] Etxebarria-Elezgarai J, Alvarez-Braña Y, Garoz-Sanchez R, Benito-Lopez F, Basabe-Desmonts L. Large-Volume Self-Powered Disposable Microfluidics by the Integration of Modular Polymer Micropumps with Plastic Microfluidic Cartridges. *Industrial & Engineering Chemistry Research*, 2020; 59: 22485-22491. <https://doi.org/10.1021/acs.iecr.0c03398>
- [22] Zimmermann M, Hunziker P, Delamarche E. Valves for autonomous capillary systems. *Microfluidics and Nanofluidics*, 2008; 5: 395-402. <https://doi.org/10.1007/s10404-007-0256-2>
- [23] Juncker D, Schmid H, Drechsler U, Wolf H, Wolf M, Michel B, de Rooij N, Delamarche E. Autonomous microfluidic capillary system, *Analytical Chemistry*, 2002; 74: 6139 - 6144. <https://doi.org/10.1021/ac0261449>
- [24] Bhattacharya S, Datta A, Berg JM, Gangopadhyay S. Studies on surface wettability of poly(dimethyl) siloxane (PDMS) and glass under oxygen-plasma treatment and correlation with bond strength. *Journal of Microelectromechanical Systems*, 2005; 14: 590-597. <https://doi.org/10.1109/JMEMS.2005.844746>

- [25] Xiang Z, Wang H, Pastorin G, Lee C. development of a flexible and disposable microneedle-fluidic-system with finger-driven drug loading and delivery functions for inflammation treatment. *Journal of Microelectromechanics*, 2015; 24: 565-574. <https://doi.org/10.1109/JMEMS.2015.2429675>
- [26] Narayanamurthy V, Jeroish ZE, Bhuvaneshwari KS, Bayat P, Premkumar R, Samsuri F, Yusoff MM. Advances in passively driven microfluidics and lab-on-chip devices: a comprehensive literature review and patent analysis. *RSC Advances*, 2020; 10:11652-80. <https://doi.org/10.1039/D0RA00263A>
- [27] Olanrewaju AO, Robillard A, Dagher M, Juncker D. Autonomous microfluidic capillary circuits replicated from 3D-printed molds. *Lab on a Chip*, 2016; 16:3804-14. <https://doi.org/10.1039/C6LC00764C>
- [28] Dimov IK, Basabe-Desmonts L, Garcia-Cordero JL, Ross BM, Ricco AJ, Lee LP. Stand-alone self-powered integrated microfluidic blood analysis system (SIMBAS). *Lab on a Chip*, 2011; 11:845-50. <https://doi.org/10.1039/C0LC00403K>
- [29] Jang I, Carrão DB, Menger RF, Moraes de Oliveira AR, Henry CS. Pump-free microfluidic rapid mixer combined with a paper-based channel. *ACS sensors*, 2020; 5:2230-8. <https://doi.org/10.1021/acssensors.0c00937>
- [30] Coskun AF, Wong J, Khodadadi D, Nagi R, Tey A, Ozcan A. A personalized food allergen testing platform on a cellphone. *Lab on a Chip*, 2013;13:636-40. <https://doi.org/10.1039/C2LC41152K>
- [31] Shen L, Hagen JA, Papautsky I. Point-of-care colorimetric detection with a smartphone. *Lab on a Chip*, 2012;12:4240-3. <https://doi.org/10.1039/c2lc40741h>
- [32] García A, Erenas MM, Marinetto ED, Abad CA, de Orbe-Paya I, Palma AJ, Capitán-Vallvey LF. Mobile phone platform as portable chemical analyzer. *Sensors and Actuators B: Chemical*. 2011;156:350-9. <https://doi.org/10.1016/j.snb.2011.04.045>
- [33] Fang X, Chen H, Jiang X, Kong J. Microfluidic devices constructed by a marker pen on a silica gel plate for multiplex assays. *Analytical Chemistry*. 2011;83:3596-9. <https://doi.org/10.1021/ac200024a>
- [34] Carrilho E, Phillips ST, Vella SJ, Martinez AW, Whitesides GM. Paper microzone plates. *Analytical Chemistry*. 2009;81:5990-8. <https://doi.org/10.1021/ac900847g>
- [35] Teasdale PR, Hayward S, Davison W. In situ, high-resolution measurement of dissolved sulfide using diffusive gradients in thin films with computer-imaging densitometry. *Analytical Chemistry*. 1999;71:2186-91. <https://doi.org/10.1021/ac981329u>

Supplementary information



Supplementary image S1. Fabrication process of the PDMS finger-pump, and microfluidic platform by soft lithography. (a) Schematic diagram of all steps necessary for the realization of the device propose. (b) The PDMS mixture is poured in the 3D mould, cured, peeled off from the mould, then cut by a razor blade.